PERGAMON

International Journal of Heat and Mass Transfer 44 (2001) 2809–2825

International Journal of HEAT and MASS TRANSFER

www.elsevier.com/locate/ijhmt

Minimum thickness of a flowing down liquid film on a vertical surface

Mohamed S. El-Genk *, Hamed H. Saber

Farris Engineering Center, Institute for Space and Nuclear Power Studies and Chemical and Nuclear Engineering, University of New Mexico, Room 239, Albuquerque, NM 87131-1341, USA

Received 16 March 2000; received in revised form 16 October 2000

Abstract

The minimum total energy (MTE) criteria for determining the minimum wetting rate and the minimum thickness of an isothermal, thin liquid film flowing down a vertical adiabatic surface are examined. An analytical expression of the profile of a stable liquid rivulet and of the two-dimensional velocity distribution in the rivulet developed using the Ritz method are incorporated into the MTE criterion to improve its predictions of the minimum wetting rate (MWR) and the corresponding minimum liquid film thickness (MLFT). The present predictions of the MWR and MLFT are in good agreement, to within ±10–20%, with experimental data for water and glycerol–water mixtures and with the values calculated from the MWR measurements, respectively. The accuracy of the present predictions is demonstrated for three conditions, namely: (a) incipient breakup of liquid film, (b) formation of a stable dry patch, and (c) rewetting of a dry surface. For the latter the advancing contact angle is substituted for the equilibrium contact angle in the developed analytical expressions for the MLFT and corresponding MWR.

Keywords: Thin liquid film; Breakup; Minimum total energy criterion; Minimum wetting rate; Contact angle; Binary mixtures

1. Introduction

The flow of isothermal, thin liquid films down vertical and inclined surfaces is encountered in many industrial applications. Examples include distillation industry, closed two-phase thermosyphons, wetted columns, cooling towers, heat exchangers, distillation, and cooling of nuclear fuel elements following a loss of coolant accidents (LOCA). The conditions under which a thin liquid film falling down a vertical or an inclined surface breaks up into a series of stable rivulets leaving the underlying surface partially dry are important to these applications. The formation of large stable dry patches and flowing rivulets on heated and unheated surfaces, following the breakup of a continuous liquid film, has been observed experimentally [1–4] (Fig. 1(a)). Several experimental investigations and mathematical approaches have been reported, respectively, for measuring and predicting the minimum wetting rate (MWR) and the corresponding minimum liquid film thickness (MLFT) for a stable dry patch (Fig. 1). Little data and modeling have been reported on the values of MWR and MLFT at the breakup of a thin liquid film and the rewetting of a previously dry surface [2]. For the former, *the MWR is the lowest flow rate needed to ensure that the surface remains covered by a continuous, thin liquid film.*

Hartely and Murgatroyd [5] have proposed the force balance (FB) at a stagnation point of a stable dry patch as a criterion for predicting the MLFT, assuming it the same as far upstream of the stagnation point (Fig. 1(b)). The MLFT is solely dependent on the equilibrium contact angle. The corresponding MWR determined based on the Nusselt theory approximation is proportional to MLFT raised to the third power (Table 1). Although the FB criterion accounts for the contact angle, θ_o, it neither accounts for the profile of the L–V interface near the stagnation point, $\phi(z)$ (Fig. 1(b)), nor ensures that the area of the liquid film enclosed by $\phi(z)$ is minimum. Consequently, the predictions of the FB

* Corresponding author. Tel.: +1-505-277-5442; fax: +1-505-277-2814.

E-mail address: mgenk@unm.edu (M.S. El-Genk).

0017-9310/01/$ - see front matter
PII: S0017-9310(00)00326-4

Nomenclature

$a_{1,2}$	coefficient (Eqs. (40a), (40b))
b	rivulet half-width (m), coefficient (Eq. (22a))
c	coefficient (Eqs. (19a), (36))
e	energy (J m^{-1})
E	dimensionless energy ($= e/(\sigma_{LV}b)$)
g	acceleration of gravity (m s^{-2})
l	length (m), coefficient (Eq. (22a))
k	curvature (m^{-1}) (Eq. (23))
K	dimensionless curvature (Eq. (38b))
p	pressure (N m^{-2})
q	volumetric flow rate (m^3 s^{-1})
Q	dimensionless flow rate ($= q\mu_l/(\rho_l g b\delta^3)$)
r	radius of curvature (m)
s	length along rivulet profile (m)
u	velocity (m s^{-1})
U	dimensionless velocity ($= u\mu_l/(g\rho_l\delta^2)$)
x	coordinate along surface (m)
X	dimensionless distance along solid surface ($= x/b$)
y	coordinate perpendicular to surface (m)
Y	dimensionless height ($= y/\delta$)
z	coordinate in direction of flow (m)

Greek symbols

α	damping coefficient (Eq. (20))
β	dimensionless coefficient (Eq. (37b))
δ	liquid film thickness (m)
Δ	dimensionless film thickness ($= \delta(\rho_l^3 g^2/15\mu_l^2\sigma_{LV})^{0.2}$)
ε	dimensionless parameter ($= (\delta/b)^2$)
Ψ	dimensionless parameter (Eq. (31))
γ	mass flow rate per unit perimeter ($= \rho_l q/2b$) (kg m^{-1} s^{-1})
Γ	dimensionless flow rate per unit perimeter ($= \gamma/(\rho_l\mu_l\sigma_{LV}^3/g)^{1/5}$)
η	approximation function (Eq. (19a))
λ	Lagrange multiplier (Eq. (32))
ϕ	rivulet profile (m)
Φ	dimensionless rivulet profile ($= \phi/\delta$)
θ	contact angle (°)
ω	dimensionless coefficient (Eq. (37a))
Ω	test function (Eq. (17))
ρ	density (kg m^{-3})
μ	dynamic viscosity (N s m^{-2})
σ	surface tension (N m^{-1})

Subscripts

0	zero-order approximation
1	first-order approximation
A	advancing
k	kinetic energy
l	liquid
min	minimum
LS	liquid–solid interface
LV	liquid–vapor interface
o	equilibrium
dR	dynamic receding
SV	solid–vapor interface
tot	total
v	vapor
σ	interfacial

Abbreviations

FB	force balance
MLFT	minimum film thickness ($= \Delta_{min}$)
MTE	minimum total energy
MWR	minimum wetting rate ($= \Gamma_{min}$)

criterion of MWR and the MLFT are 40–70% and 30% higher than the measurements and the values determined from the MWR measurements, respectively.

Hobler [6] has introduced the criterion of minimum total energy (MTE) to determine the MLFT for a stable dry patch by minimizing the total energy of a flowing liquid rivulet (Figs. 1 and 2). The minimum total energy (MTE) criterion states that if the total energy in a given streamwise length of a liquid rivulet is minimum, the rivulet will breakup. Otherwise, the continuous liquid rivulet is stable and no further breakup occurs. This criterion argues for the notion that the minimum liquid film thickness determined based on MTE also applies to the breakup of a continuous, thin liquid film falling down a vertical or an inclined surface. The validity of this opinion is investigated in this work. In addition, the application of the MTE to predict the MLFT and the corresponding MWR for rewetting a previously dry patch are investigated. Although the MTE criterion accounts for the contact angle (Table 1 and Fig. 2), its accuracy depends on the accurate determination of the profile of the rivulet, $\phi(x)$, as well as the velocity distribution within the rivulet, $u_l(x, y)$.

Some investigators have assumed a rivulet profile that is a segment of a circle [7,8]. This assumption, however, requires the contact angle at the triple point to change with the dimensions of the rivulet, as a result of increasing or decreasing of the liquid mass flow rate. Doniec [9] determined the profile, $\phi(x)$, for a symmetrical waveless rivulet, from the numerical solution of the MTE equation. However, he did not use the rivulet profile in deriving an expression for the minimum wetting rate, Γ_{min}. Instead, Γ_{min} has been determined using the Nusselt theory approximation.

In all other reported work on MTE criterion, the velocity distribution in the liquid rivulet has been de-

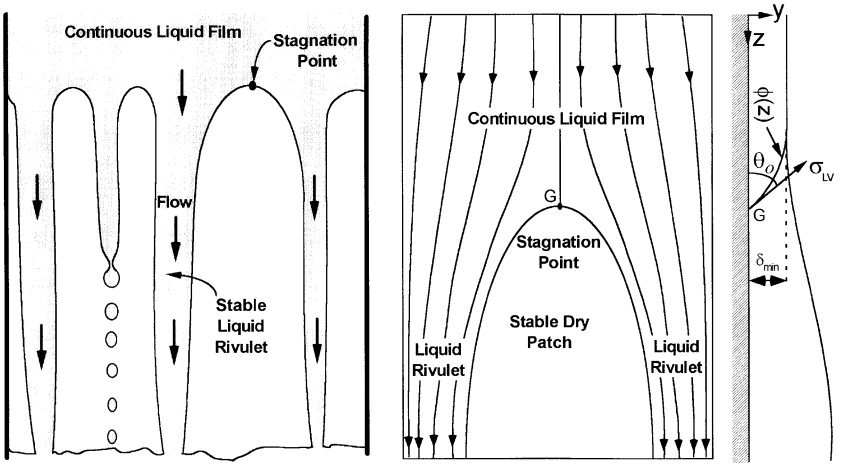

(a) Observed breakup of liquid film in a two-phase thermosyphon [3]

(b) A schematic of a stable dry patch

Fig. 1. A stable dry patch, following the breakup of a thin liquid film flowing down an vertical surface.

Table 1
Reported analytical expressions of the MLFT and the MWR for a stable dry patch

Reference	Reported equations	Comments
[5]	$\Delta_{\min} = (1-\cos\theta_o)^{1/5}$	• FB at stagnation point • MLFT same as far upstream of stagnation point
	$\Gamma_{\min} = 1.693\Delta_{\min}^3$	• Zero-order velocity approximation
[6]	$\Delta_{\min} = (3/2)^{1/5}(1-\cos\theta_o)^{1/5}$	• MTE of liquid rivulet • No information on rivulet profile • Zero-order velocity approximation
[7,8]	$\Delta_{\min}^5 + (1-\cos\theta_o) - G(\theta_o)\Delta_{\min}^3 = 0$	• MTE of liquid rivulet • Assumed a circular rivulet profile • Zero-order velocity approximation
	$\Gamma_{\min}$ (derived) $= 1.693\Delta_{\min}^3$	• Derived expression for $\Gamma_{\min}$ from Nusselt theory approximation
[9]	$\Delta_{\min} = (3/7)^{1/5}(1-\cos\theta_o)^{1/5}$ $\Gamma_{\min} = 1.693\Delta_{\min}^3$	• MTE of liquid rivulet • Determined the rivulet profile from numerical solution of the MTE equation • Zero-order velocity approximation • Derived expression for $\Gamma_{\min}$ from Nusselt theory approximation

Here

$$G(\theta_o) = \left(\frac{5}{2}\right)\frac{\sin\theta_o}{f(\theta_o)}\left(\frac{2\psi(\theta_o)}{3\sin\theta_o}\right)^{3/5}\left(\frac{\theta_o}{\sin\theta_o}-\cos\theta_o\right)^{2/5}$$

$$f(\theta_o) = -\frac{1}{4}\cos^3\theta_o\sin\theta_o - \frac{13}{8}\cos\theta_o\sin\theta_o - \frac{3}{2}\theta_o\sin^2\theta_o + \frac{15}{8}\theta_o$$

and

$$\psi(\theta_o) = \theta_o\left(\frac{5}{16}+\frac{15}{4}\cos^2\theta_o+\frac{5}{2}\cos^4\theta_o\right) - \sin\theta_o\left(\frac{113}{48}\cos\theta_o+\frac{97}{24}\cos^3\theta_o+\frac{1}{6}\cos^5\theta_o\right)$$

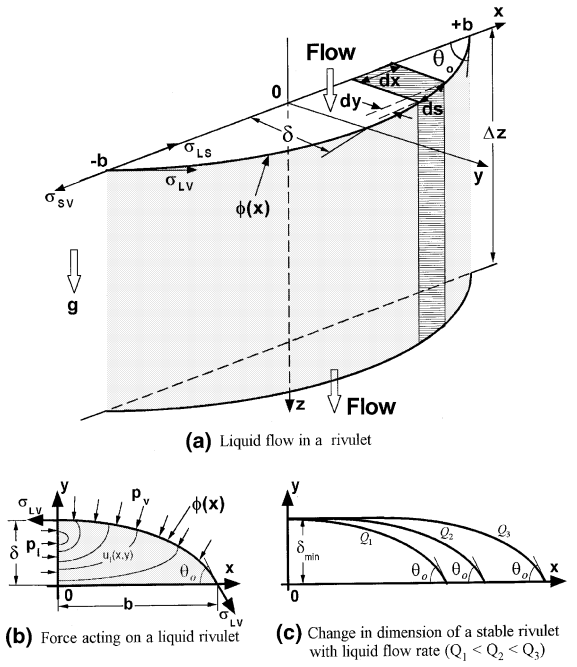

Fig. 2. A stable liquid rivulet flowing down an isothermal vertical wall.

scribed by a zero-order approximation of a power series representation of the liquid velocity [6–9]. While this velocity distribution is reasonable at small contact angles (<20°), it deviates progressively from the exact solution as the contact angle increases. As with the FB criterion [5], the MWR in the MTE criterion has been derived based on the Nusselt theory approximation [6–9]. Consequently the relationship for MWR as a function of MLFT is the same for all reported work on FB and MTE criteria (Table 1). Figs. 3(a)–(c) compare the expressions of the MWR in Table 1 with reported measurements of water for a stable dry patch [1].

As shown in Fig. 3(a), the FB criterion [5] over estimates the MWR for water by as much as 70%, while the predictions of the MTE criterion based on Doniec's [9] approach over predicts the data by 50% (Fig. 3(b)). The MTE criterion, based on the approach of Mikielewicz and Moszynski [8], however, underestimates the MWR by 230% (Fig. 3(c)). Fig. 3(d) compares the various expressions of the MLFT in Table 1 versus the equilibrium contact angle. Based on this comparison, it is difficult to draw a conclusion regarding the applicability of the MTE criterion. However, using accurate expressions for the liquid velocity distribution in the rivulet, $u_l(x,y)$, and of the rivulet profile could improve the comparison of the MTE criterion with data. This issue is investigated in this paper.

The developed analytical expressions for the MLFT and the corresponding MWR are based on the MTE criterion. The total energy of a stable liquid rivulet (Figs. 1 and 2) is taken as the sum of the kinetic and interfacial energies. The latter includes the energies at the liquid–gas (L–V) and the liquid-solid (L–S) interfaces. To determine the kinetic energy, e_k, at a given liquid flow rate, q, an approximate analytical expression for the velocity distribution, $u_l(x,y)$ in the liquid rivulet is obtained using the Ritz Method [10]. The obtained expression for $u_l(x,y)$ is compared with the numerical solution of Allen and Biggin [11] for the same rivulet profile.

The present predictions of the MWR are compared with the reported measurements of water for a stable dry patch at contact angles of 66°–87°. In addition, the applicability of these predictions to the breakup of a continuous, thin liquid film of water and glycerol–water mixtures and for rewetting a dry patch is examined. To determine the accuracy of the present expression for the MLFT, predictions are compared with the values calculated from the reported measurements of the MWR for water and glycerol–water mixtures.

2. Energy equations

Following the breakup of a continuous liquid film flowing down a vertical or inclined surface, stable liquid rivulets form, separated by dry patches (Fig. 1). The liquid flow in a rivulet forms a free surface whose shape depends on the liquid flow rate (Figs. 2(b) and (c)). The curve created by the intersection of the surface perpendicular to the direction of the liquid flow in the rivulet with the free surface or L–V interface is the rivulet's profile, $\phi(x)$. This profile intersects the underlying solid surface (Fig. 2(b)). The tangent to the rivulet profile at the triple points of the gas, solid, and liquid phases determines the equilibrium contact angle, θ_o, a measure of the interrelationships between the surface forces of the solid, liquid, and gas phases. Thus, this angle appears in the relation between the interfacial energies at the L–V, L–S and S–V interfaces.

For a stable, symmetrical liquid rivulet (Fig. 2(b)), the total energy is the sum of the kinetic energy, e_k, and the interfacial energies, e_σ. The infinitesimal kinetic energy, de_k, per unit length of the rivulet is given as

$$de_k = \left(\int_0^{\phi} \frac{\rho_l}{2} u_l^2(x,y)\, dy \right) dx. \tag{1}$$

The interfacial energy per unit length, e_σ, is the sum of those at the L–V interface, $de_{\sigma,LV}$ and at the L–S interface, $de_{\sigma,LS}$. The infinitesimal interfacial energy at the L–V interface is

$$de_{\sigma,LV} = \sigma_{LV}\, ds, \tag{2}$$

where

$$ds = dx\sqrt{1 + (d\phi(x)/dx)^2}. \tag{3}$$

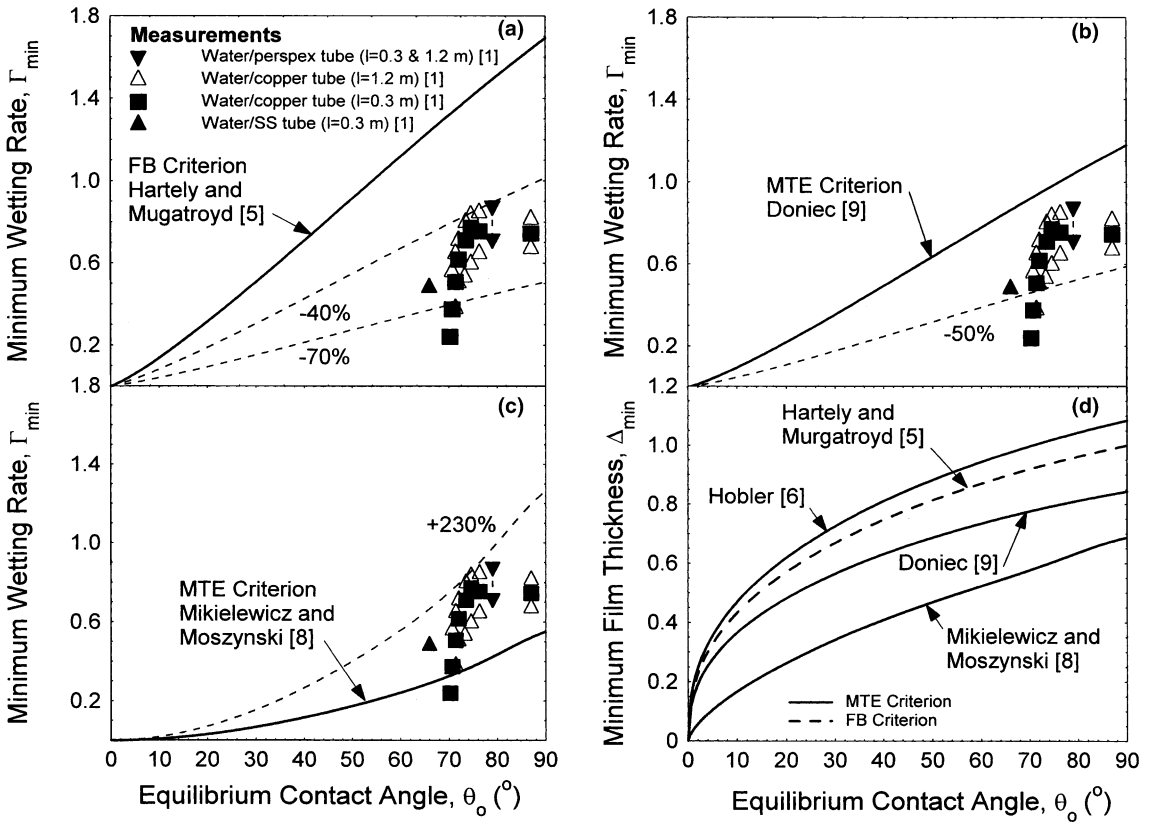

Fig. 3. Comparison of the various expressions of MWR and MLFT for a stable dry patch of water.

Substituting Eq. (3) into Eq. (2) give the infinitesimal interfacial energy at L–V interface:

$$de_{\sigma,\mathrm{LV}} = \sigma_{\mathrm{LV}}\sqrt{1+(d\phi(x)/dx)^2}\,dx. \tag{4}$$

The interfacial energy at the L–S interface is

$$de_{\sigma,\mathrm{LS}} = \sigma_{\mathrm{LS}}\,dx. \tag{5}$$

From the force balance at the triple point (Fig. 2(b)), the surface tension at the L–S interface, σ_{LS}, is written in terms of σ_{SV}, σ_{LV}, and the equilibrium contact angle, θ_{o}, as

$$\sigma_{\mathrm{LS}} = \sigma_{\mathrm{SV}} - \sigma_{\mathrm{LV}}\cos\theta_{\mathrm{o}}. \tag{6}$$

Substituting Eq. (6) into Eq. (5) gives the infinitesimal energy at the L–S interface as

$$de_{\sigma,\mathrm{LS}} = (\sigma_{\mathrm{SV}} - \sigma_{\mathrm{LV}}\cos\theta_{\mathrm{o}})\,dx. \tag{7}$$

Eqs. (1), (4) and (7) gives the total energy per unit length of the rivulet as

$$e_{\mathrm{tot}} = 2\int_0^b \left[\left(\int_0^\phi \frac{\rho_{\mathrm{l}}}{2}u_{\mathrm{l}}^2(x,y)\,dy\right) + \left(\sigma_{\mathrm{LV}}\sqrt{1+(d\phi/dx)^2} - \sigma_{\mathrm{LV}}\cos\theta_{\mathrm{o}} + \sigma_{\mathrm{SV}}\right)\right]dx. \tag{8}$$

The volumetric flow rate depends on the profile of the rivulet $\phi(x)$ (Fig. 2(b)) as

$$q = \int_0^b q'\,dx, \tag{9a}$$

where

$$q' = 2\int_0^\phi u_{\mathrm{l}}(x,y)\,dy. \tag{9b}$$

The liquid velocity distribution, $u_{\mathrm{l}}(x,y)$ in the rivulet, required to evaluate the total energy, e_{tot} (Eq. (8)) and the liquid volumetric flow rate, q (Eqs. (9a), (9b)), is obtained in the following section.

3. Velocity distribution in liquid rivulet

For a steady, incompressible, and Newtonian liquid flowing down a solid surface (Fig. 2(a)), the momentum equations are:

$$\frac{\partial p_{\mathrm{l}}}{\partial x} = 0, \quad \frac{\partial p_{\mathrm{l}}}{\partial y} = 0 \tag{10a}$$

and

$$\frac{\partial^2 u_l(x,y)}{\partial x^2}+\frac{\partial^2 u_l(x,y)}{\partial y^2}=-\frac{g\rho_l}{\mu_l}. \tag{10b}$$

Eq. (10b) is subject to the boundary conditions:

$$u_l(x,0)=0,\quad \frac{\partial u_l(0,y)}{\partial x}=0, \tag{11a}$$

and a zero shear stress at the L–V interface ($y=\phi(x)$):

$$-\phi'(x)\frac{\partial u_l(x,\phi)}{\partial x}+\frac{\partial u_l(x,\phi)}{\partial y}=0. \tag{11b}$$

The liquid velocity $u_l(x,y)$ has been expressed as a power series of the form [11]

$$u(x,y)=u_{00}+\varepsilon u_{11}+\varepsilon^2 u_{22}+\varepsilon^3 u_{33}+\cdots \tag{12}$$

In this expression, $u_0=u_{00}$ and $u_1=u_{00}+\varepsilon u_{11}$ are the zero- and first-order approximations of the velocity distribution in the liquid rivulet, respectively. Substituting Eq. (12) into Eqs. (10b) and (11a), (11b) and solving for the zero-order velocity approximation, u_0, subject to the condition $\partial^2 u_l(x,y)/\partial x^2=0$ gives [11]

$$u_0=\frac{g\rho_l}{\mu_l}\left(y\phi-\frac{1}{2}y^2\right). \tag{13}$$

This velocity distribution, which is same as that of the Nusselt theory approximation, has been used to determine the MWR by the investigators [5–9] listed in Table 1. Similarly, the first-order approximation of the velocity distribution, $u_1(x,y)$ is obtained, subject to the condition $u_1=u_{00}+\varepsilon u_{11}$ and $u_{22}=u_{33}=\cdots=0$, as

$$u_1=\frac{\rho_l g}{\mu_l}\left(y\phi-\frac{1}{2}y^2+y\phi\phi'^2+\frac{1}{2}y\eta^2\phi''-\frac{1}{6}y^3\phi''\right). \tag{14}$$

3.1. Determination of the velocity distribution using Ritz method

Eq. (10b), subject to the boundary conditions given by Eqs. (11a) and (11b) represents a nonlinear problem. Since, this problem does not have an analytical solution, the Ritz method [10] is used to obtain an approximate analytical expression for the 2D velocity distribution in the liquid rivulet. Eq. (10b) and the boundary conditions in Eqs. (11a) and (11b) are expressed in a dimensionless form as

$$\varepsilon\frac{\partial^2 U_l(X,Y)}{\partial X^2}+\frac{\partial^2 U_l(X,Y)}{\partial Y^2}=-1, \tag{15}$$

$$U_l(X,0)=0, \tag{16a}$$

$$\frac{\partial U_l(0,Y)}{\partial X}=0 \tag{16b}$$

and

$$-\varepsilon\Phi'(X)\frac{\partial U_l(X,\Phi)}{\partial X}+\frac{\partial U_l(X,\Phi)}{\partial Y}=0. \tag{16c}$$

The weak or variational formulation of Eq. (15) is constructed by multiplying both sides of this equation by a test function Ω and integrating over the domain of the liquid rivulet as

$$\int_0^1\int_0^{\Phi}\Omega\left(\varepsilon\frac{\partial^2 U_l(X,Y)}{\partial X^2}+\frac{\partial^2 U_l(X,Y)}{\partial Y^2}+1\right)\mathrm{d}Y\,\mathrm{d}X=0. \tag{17}$$

After performing the above integration and using the boundary conditions in Eqs. (16b) and (16c), the weak formulation becomes

$$\int_0^1\int_0^{\Phi}\left(\varepsilon\frac{\partial\Omega}{\partial X}\frac{\partial U_l}{\partial X}+\frac{\partial\Omega}{\partial Y}\frac{\partial U_l}{\partial Y}\right)\mathrm{d}Y\,\mathrm{d}X=\int_0^1\int_0^{\Phi}\Omega\,\mathrm{d}Y\,\mathrm{d}X. \tag{18}$$

The Ritz method seeks an approximate velocity distribution in the form of a finite series as

$$U(X,Y)=\eta_0+\sum_{i=1}^{m}c_i\eta_i(X,Y). \tag{19a}$$

The selected function η_0, should satisfy the primary variable boundary condition Eq. (16a), thus in the present problem, η_0 is 0, therefore:

$$U(X,Y)=\sum_{i=1}^{m}c_i\eta_i(X,Y). \tag{19b}$$

The requirements for selecting the approximation functions, η_i $(i=1,2,\ldots,m)$, are described in detail by Reddy [10] and will not be repeated here. For determining the velocity distribution in the liquid rivulet, η_i is assumed to have the form

$$\eta_i=\cos\frac{(2i-1)\alpha}{2}X\sin i\alpha Y. \tag{20}$$

The coefficient α, referred to as "*damping coefficient*", plays an effective role in reducing the number of terms required to accurately express the velocity distribution (Eq. (19b)). A value of $\alpha=0.05$ is found adequate to obtain an accurate velocity distribution in the liquid rivulet using only three terms ($m=3$) in Eq. (19b).

The coefficients c_i $(i=1,2,\ldots,m)$ in Eq. (19b) called Ritz coefficients are chosen such that Eq. (18) holds for the test function $\Omega=\eta_i$ $(i=1,2,\ldots,m)$, thus Eq. (18) becomes

$$\int_0^1 \int_0^{\Phi} \left(\varepsilon \frac{\partial \eta_i}{\partial X} \sum_{j=1}^{m} c_j \frac{\partial \eta_j}{\partial X} + \frac{\partial \eta_i}{\partial Y} \sum_{j=1}^{m} c_j \frac{\partial \eta_j}{\partial Y} \right) \mathrm{d}Y \, \mathrm{d}X = \int_0^1 \int_0^{\Phi} \eta_j \, \mathrm{d}Y \, \mathrm{d}X, \quad i = 1, 2, \ldots, m. \tag{21}$$

The above equation can be written in the matrix form as

$$\begin{bmatrix} b_{11} & b_{12} & \cdots & b_{1n} \\ b_{21} & b_{22} & \cdots & b_{2n} \\ \vdots & \vdots & \vdots & \vdots \\ b_{n1} & b_{n2} & \cdots & b_{nn} \end{bmatrix} \begin{Bmatrix} c_1 \\ c_2 \\ \vdots \\ c_n \end{Bmatrix} = \begin{Bmatrix} l_1 \\ l_2 \\ \vdots \\ l_n \end{Bmatrix}, \tag{22a}$$

where

$$b_{ij} = \int_0^1 \int_0^{\Phi} \left(\varepsilon \frac{\partial \eta_i}{\partial X} \frac{\partial \eta_j}{\partial X} + \frac{\partial \eta_i}{\partial Y} \frac{\partial \eta_j}{\partial Y} \right) \mathrm{d}Y \, \mathrm{d}X$$
$$l_i = \int_0^1 \int_0^{\Phi} \eta_i \, \mathrm{d}Y \, \mathrm{d}X. \tag{22b}$$

The coefficients c_i $(i = 1, 2, \ldots, m)$ in Eq. (19b) are determined from the solution of the set of linear algebraic equations in Eq. (22a), where the integrals in Eq. (22b) are evaluated numerically. In order to evaluate these integrals, however, the surface profile of the rivulet, $\Phi(X)$, needs to be determined. The rivulet's profile is a complex function of the equilibrium contact angle, θ_o, the width, b, and the height, δ, of the rivulet (Fig. 2(b)), and the velocity distribution in the rivulet, $u_l(x, y)$.

4. Rivulet profile

According to Eq. (10a), $p_l(x) = p_l$, thus the liquid pressure of the liquid rivulet is independent of x. The relationship between p_l and p_v is described by the Laplace relation:

$$p_l - p_v = \sigma_{LV} k, \quad \text{where } k = -\frac{\phi''(x)}{\left(1 + \phi'^2(x)\right)^{3/2}}. \tag{23}$$

The force balance at the L–V interface of the liquid rivulet (see Fig. 2(b)) is given as

$$p_l - p_v = \frac{\sigma_{LV}}{\delta}(1 - \cos\theta_o). \tag{24}$$

Substituting Eq. (23) into Eq. (24), gives a nonlinear, second-order, ordinary differential equation for the surface profile of the liquid rivulet as

$$\frac{\phi''(x)}{(1 + \phi'^2(x))^{3/2}} = -\frac{(1 - \cos\theta_o)}{\delta}. \tag{25}$$

Eq. (25) is solved analytically for $\phi(x)$ using the boundary conditions:

$$\phi(x = 0) = \delta \quad \text{and} \quad \phi'(x = 0) = 0, \tag{26a}$$
$$\phi(x = b) = 0 \quad \text{and} \quad \phi'(x = b) = -\tan\theta_o. \tag{26b}$$

The obtained expression for the rivulet profile, $\phi(x)$, is as follows:

$$\phi(x) = \delta - \frac{\delta}{(1 - \cos\theta_o)} \times \left\{ 1 - \sqrt{1 - x^2 \left(\frac{1 - \cos\theta_o}{\delta} \right)^2} \right\}. \tag{27}$$

Eq. (27) is rewritten in a dimensionless form as

$$\Phi(X) = 1 - \frac{1}{(1 - \cos\theta_o)} \times \left\{ 1 - \sqrt{1 - \frac{X^2}{\varepsilon}(1 - \cos\theta_o)^2} \right\}. \tag{28}$$

As this equation indicates, the rivulet profile can be characterized by the equilibrium contact angle, θ_o, and the aspect ratio, ε, of the liquid rivulet. These values are varied when comparing the present velocity distribution, $U_l(X, Y)$, with the zero- and first-order velocity approximations (Eqs. (13) and (14)) in the next section. The values of $U_l(X, Y)$ are obtained by solving Eqs. (19b), (20), (22a), (22b) and (28).

4.1. Validation of present velocity distribution in liquid rivulet

The present expression of the velocity distribution in the rivulet (Eqs. (19b) and (20)) is compared in Fig. 4 with the numerical solution of Allen and Biggin [11] for the same rivulet profile characterized by $\theta_o = 45°$ and

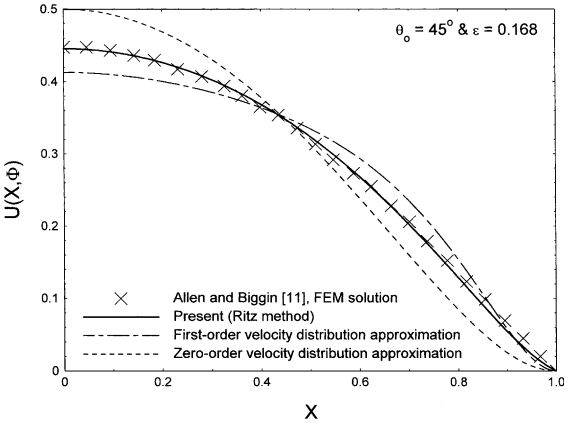

Fig. 4. Comparison of the present velocity distribution at L–V interface with the numerical solution [11].

$\varepsilon = 0.168$. Fig. 4 shows excellent agreement between the present velocity distribution at the L–V interface of the rivulet and the numerical solution of Allen and Biggin [11] obtained using finite element method (FEM). The zero- and the first-order approximations of the velocity distribution, however, deviate from the present and the FEM solutions at the center of the rivulet ($X = 0$) by $+12.3\%$ and -7.3%, respectively. Unlike the present expression for the velocity distribution in the rivulet, the numerical solution of Allen Biggin [11] cannot be incorporated into the total energy (Eq. (8)) to derive expression for the MLFT based on MTE.

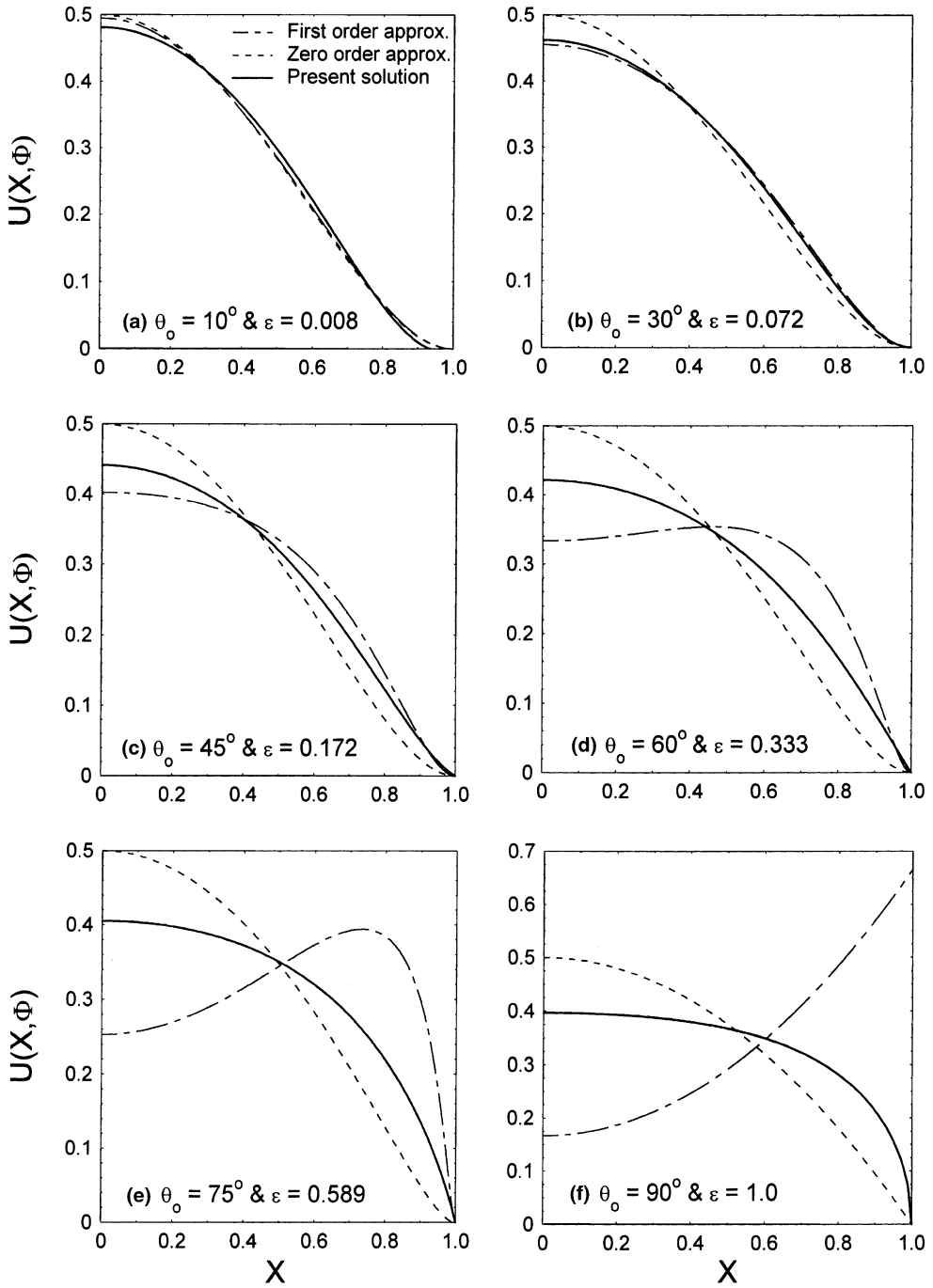

Fig. 5. Comparison of zero- and first-order velocity approximations with the present solution (Eq. (19b)).

For a rivulet profile characterized by a small contact angle, $\theta_o = 10°$, and $\varepsilon = 0.008$, both the zero-order, U_0, and first-order, U_1, velocity approximations are close to the present solution (Fig. 5(a)). For a rivulet profile having $\theta_o = 30°$ and $\varepsilon = 0.072$, the first-order velocity approximation remains close to the present solution, however, the zero-order approximation deviates from the present solution at the center of the rivulet ($X = 0$) by ~8.2% (Fig. 5(b)). As the contact angle and ε increase, the deviation of both the zero- and first-order velocity approximations from the present velocity distribution in the rivulet increases. For example, for a

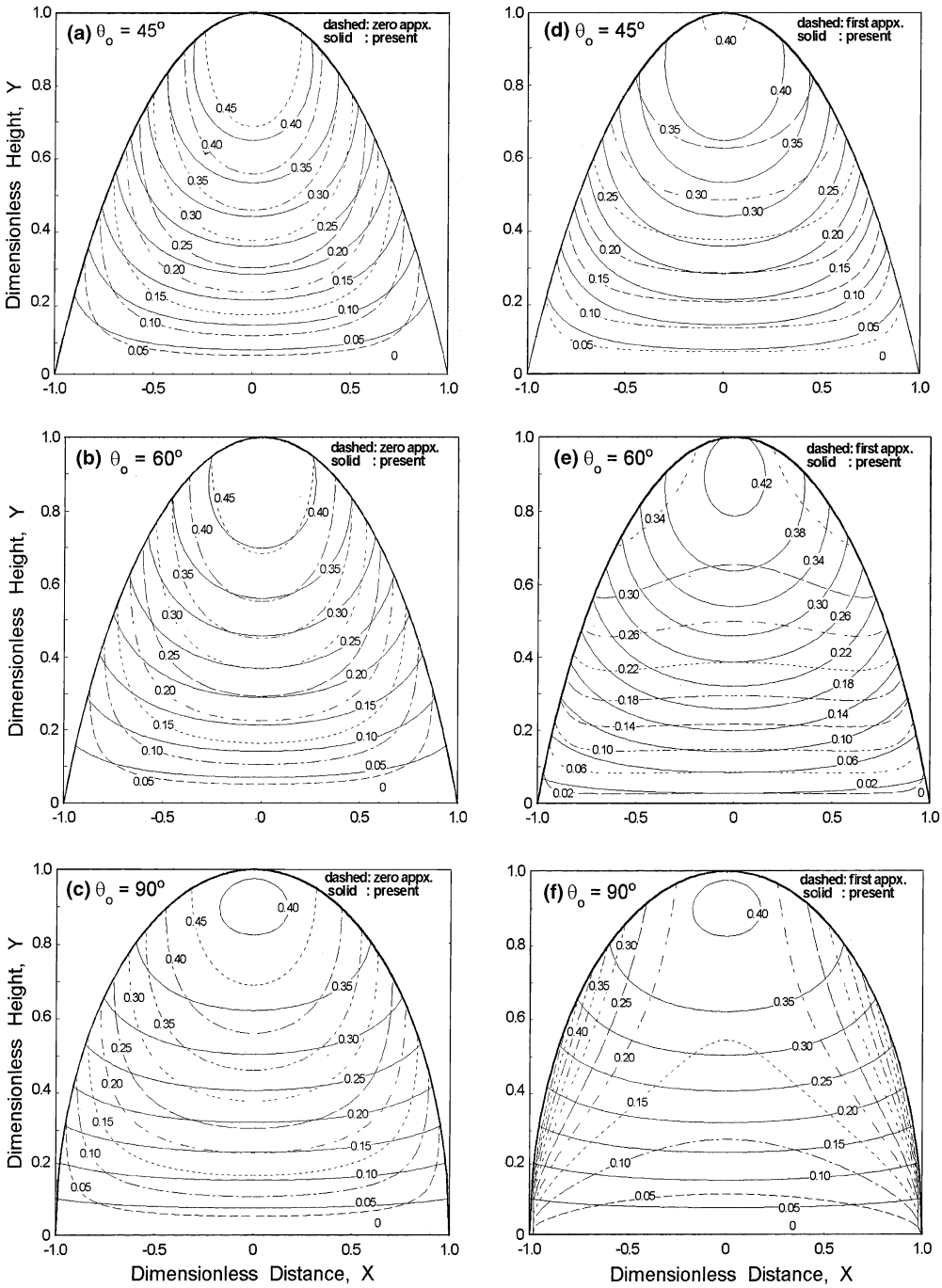

Fig. 6. Comparisons of the calculated velocity contour lines within a stable liquid rivulet.

rivulet profile having $\theta_o = 45°$ and $\varepsilon = 0.172$, the zero- and first-order velocity approximations deviate from the present velocity distribution at the center of the rivulet by -8.8% to $+13.3\%$ (Figs. 5(c) and 6(a), (d)). The deviation increases to -20.9% and $+18.6\%$ when $\theta_o = 60°$ and $\varepsilon = 0.333$ (Figs. 5(d) and 6(b), (e)). When $\theta_o = 75°$ and $\varepsilon = 0.589$, the first-order velocity approximation becomes unstable, while the zero-order velocity approximation deviates from the present velocity distribution at $X = 0$ and $X = 0.8$ by as much as -41.2% to $+23.4\%$, respectively (Fig. 5(e)).

Figs. 6(a)–(f) compare the contour lines of the present velocity distribution obtained using the Ritz method (solid lines) with those of the zero- and first-order velocity approximations (dashed lines). As shown in these figures, both the zero- and first-order velocity approximations deviate from the present velocity distribution, with the deviation becoming significant as the contact angle increases. Therefore, the zero-order, and certainly the first-order, velocity approximation is not accurate enough to determine the velocity distribution in the liquid rivulet as a function of the equilibrium contact angle, θ_o, and ε. In addition, the instability of the first-order velocity approximation for $\theta_o \geqslant 60°$ argues for avoiding its use entirely.

In the next section, the velocity distribution obtained using the Ritz method (Eq. (19b)) is incorporated into Eqs. (8) and (9a), (9b) to determine the profile of the liquid rivulet and, hence, obtain analytical expressions for the MLFT and MWR from the minimization of the total energy (Eq. (8)).

5. Total energy minimization

As indicated earlier, when $\alpha = 0.05$ only three terms in the finite series in Eq. (19b) are sufficient to describe the velocity distribution in the liquid rivulet as

$$U(X,Y) = \sum_{i=1}^{3} c_i \cos\frac{(2i-1)\alpha}{2} X \sin i\alpha Y. \tag{29}$$

Substituting Eq. (29) into Eq. (8) and integrating with respect to Y, gives the dimensionless total energy of the liquid rivulet as

$$E = \int_0^1 E' \,\mathrm{d}X, \tag{30a}$$

where

$$\begin{aligned} E' = 2\Bigg\{ & \left[\frac{15}{2}\Delta^5 \left[\sum_{i=1}^{3} \frac{c_i^2}{2} \cos^2 \frac{(2i-1)\alpha}{2} X \right. \right. \\ & \times \left[\Phi(X) - \frac{1}{2i\alpha} \sin 2i\alpha\Phi(X) \right] + 2\frac{c_1 c_2}{\alpha} \cos\frac{\alpha}{2} X \cos\frac{3\alpha}{2} X \\ & \times \left[\frac{1}{2}\sin\alpha\Phi(X) - \frac{1}{6}\sin 3\alpha\Phi(X) \right] + 2\frac{c_1 c_3}{\alpha} \cos\frac{\alpha}{2} X \cos\frac{5\alpha}{2} X \\ & \times \left[\frac{1}{2}\sin 2\alpha\Phi(X) - \frac{1}{8}\sin 4\alpha\Phi(X) \right] + 2\frac{c_2 c_3}{\alpha} \cos\frac{3\alpha}{2} X \cos\frac{5\alpha}{2} X \\ & \left. \left. \times \left[\frac{1}{2}\sin\alpha\Phi(X) - \frac{1}{10}\sin 5\alpha\Phi(X) \right] \right] \right] \\ & + \left(1 + \varepsilon\Phi'^2(X) \right)^{1/2} + \frac{\sigma_{SV}}{\sigma_{LV}} - \cos\theta_o \Bigg\}. \end{aligned} \tag{30b}$$

The condition to minimize the total energy of the rivulet (Eq. (30a)) is described by the Euler equation [12]:

$$\frac{\partial\Psi}{\partial\Phi} = \frac{\mathrm{d}}{\mathrm{d}X}\left(\frac{\partial\Psi}{\partial\Phi'} \right), \quad \text{where } \Phi' = \mathrm{d}\Phi(X)/\mathrm{d}X. \tag{31}$$

In this equation, Φ and Φ' are given by Eq. (28), and Ψ is given as

$$\Psi = E' + \lambda Q'. \tag{32}$$

The term E' is given by Eq. (30b), and Q' is obtained from substituting Eq. (29) into Eq. (9b) and integrating with respect to Y as

$$Q' = 2\sum_{i=1}^{3} \frac{c_i}{i\alpha} \cos\frac{(2i-1)\alpha}{2} X[1 - \cos i\alpha\Phi(X)]. \tag{33}$$

The parameter λ in Eq. (32) is the isoperimetric constant (or Lagrange multiplier). To determine this parameter, Eq. (31) is integrated once as

$$\Psi - \Phi'\left(\frac{\partial\Psi}{\partial\Phi'} \right) = c. \tag{34}$$

Substituting Eqs. (30b), (32) and (33) into Eq. (34), gives

$$\begin{aligned} & \frac{15}{2}\Delta^5 \left[\sum_{i=1}^{3} \frac{c_i^2}{2} \cos^2 \frac{(2i-1)\alpha}{2} X \right. \\ & \times \left[\Phi(X) - \frac{1}{2i\alpha} \sin 2i\alpha\Phi(X) \right] \\ & + 2\frac{c_1 c_2}{\alpha} \cos\frac{\alpha}{2} X \cos\frac{3\alpha}{2} X \\ & \times \left[\frac{1}{2}\sin\alpha\Phi(X) - \frac{1}{6}\sin 3\alpha\Phi(X) \right] \\ & + 2\frac{c_1 c_3}{\alpha} \cos\frac{\alpha}{2} X \cos\frac{5\alpha}{2} X \\ & \times \left[\frac{1}{4}\sin 2\alpha\Phi(X) - \frac{1}{8}\sin 4\alpha\Phi(X) \right] \end{aligned}$$

$$+2\frac{c_2c_3}{\alpha}\cos\frac{3\alpha}{2}X\cos\frac{5\alpha}{2}X \times\left[\frac{1}{2}\sin\alpha\Phi(X)-\frac{1}{10}\sin5\alpha\Phi(X)\right]\Bigg] +\left(1+\varepsilon\Phi'^2(X)\right)^{1/2}+\frac{\sigma_{SV}}{\sigma_{LV}}-\cos\theta_o +\lambda\sum_{i=1}^{3}\frac{c_i}{i\alpha}\cos\frac{(2i-1)\alpha}{2}X[1-\cos i\alpha\Phi(X)] -\frac{\varepsilon\Phi'^2(X)}{\left(1+\varepsilon\Phi'^2(X)\right)^{1/2}}=c. \tag{35}$$

The coefficients c and λ are then evaluated by applying the two boundary conditions given by Eqs. (26a) and (26b) to Eq. (35), which yields

$$c=\frac{\sigma_{SV}}{\sigma_{LV}},\qquad \lambda=-\left((1-\cos\theta_o)+\frac{15}{2}\Delta^5\omega\right)\Big/\beta. \tag{36}$$

The coefficients ω and β in Eq. (36) are given as

$$\omega=\sum_{i=1}^{3}c_i^2\left(\frac{1}{2}-\frac{1}{4i\alpha}\sin2i\alpha\right) +2\frac{c_1c_2}{\alpha}\left(\frac{1}{2}\sin\alpha-\frac{1}{6}\sin3\alpha\right) +2\frac{c_1c_3}{\alpha}\left(\frac{1}{4}\sin2\alpha-\frac{1}{8}\sin4\alpha\right) +2\frac{c_2c_3}{\alpha}\left(\frac{1}{2}\sin\alpha-\frac{1}{10}\sin5\alpha\right) \tag{37a}$$

and

$$\beta=\sum_{i=1}^{3}\frac{c_i}{i\alpha}(1-\cos i\alpha). \tag{37b}$$

The Euler Eq. (31) is solved for the height of the liquid rivulet at its center ($X=0$). Substituting Eq. (32) into Eq. (31), and rearranging the results give

$$\frac{\varepsilon\Phi''(X)}{\left(1+\varepsilon\Phi'^2(X)\right)^{3/2}} =\frac{15}{4}\Delta^5\Bigg(\sum_{i=1}^{3}c_i^2\cos^2\frac{(2i-1)\alpha}{2}X(1-\cos2i\alpha\Phi(X)) +2c_1c_2\cos\frac{\alpha}{2}X\cos\frac{3\alpha}{2}X[\cos\alpha\Phi(X)-\cos3\alpha\Phi(X)] +2c_1c_3\cos\frac{\alpha}{2}X\cos\frac{5\alpha}{2}X[\cos2\alpha\Phi(X)-\cos4\alpha\Phi(X)] +2c_2c_3\cos\frac{3\alpha}{2}X\cos\frac{5\alpha}{2}X[\cos\alpha\Phi(X)-\cos5\alpha\Phi(X)]\Bigg) +\lambda\sum_{i=1}^{3}c_i\cos\frac{(2i-1)\alpha}{2}X\sin i\alpha\Phi(X). \tag{38a}$$

The left-hand side of Eq. (38a) is the dimensionless local curvature, $K(X)$, of the rivulet profile, $\Phi(X)$, which is defined as

$$K(X)=\varepsilon\Phi''(X)\left(1+\varepsilon\Phi'^2(X)\right)^{-3/2}. \tag{38b}$$

Differentiating Eq. (38a) with respect to X and setting $dK(X)/dX=0$ at $X=0$, gives the rivulet height at its center, which is same as the dimensionless MLFT (or Δ_{min}), as

$$\Delta_{min}=\left(a_2(1-\cos\theta_o)\Big/\left(\beta a_1-\frac{15}{2}\omega a_2\right)\right)^{1/5}. \tag{39}$$

The coefficients ω and β are given by Eqs. (37a) and (37b), and a_1 and a_2 are given as

$$a_1=\sum_{i}^{3}c_i^2\left(2i\alpha\sin2i\alpha+2\varepsilon\left(\frac{(2i-1)\alpha}{2}\right)^2\frac{1-\cos2i\alpha}{1-\cos\theta_o}\right) +2c_1c_2\left((3\alpha\sin3\alpha-\alpha\sin\alpha)+10\varepsilon\left(\frac{\alpha}{2}\right)^2\frac{\cos\alpha-\cos3\alpha}{1-\cos\theta_o}\right) +2c_1c_3\left((4\alpha\sin4\alpha-2\alpha\sin2\alpha)+26\varepsilon\left(\frac{\alpha}{2}\right)^2\frac{\cos2\alpha-\cos4\alpha}{1-\cos\theta_o}\right) +2c_2c_3\left((5\alpha\sin5\alpha-\alpha\sin\alpha)+34\varepsilon\left(\frac{\alpha}{2}\right)^2\frac{\cos\alpha-\cos5\alpha}{1-\cos\theta_o}\right) \tag{40a}$$

and

$$a_2=\sum_{i}^{3}c_i\left(i\alpha\cos i\alpha+\varepsilon\left(\frac{(2i-1)\alpha}{2}\right)^2\frac{\sin i\alpha}{1-\cos\theta_o}\right). \tag{40b}$$

Substituting Eq. (39) into (9a) and (9b), yields the following expression for the dimensionless MWR (or Γ_{min}) as:

$$\Gamma_{min}=(15)^{3/5}(\Delta_{min})^3\int_0^1\sum_{i=1}^{3}\frac{c_i}{i\alpha}\cos\frac{(2i-1)\alpha}{2}X \times(1-\cos i\alpha\Phi(X))\,dX. \tag{41}$$

The integration in Eq. (41) is evaluated numerically. For simplicity, Eq. (39) can be expressed in terms of θ_o using the following empirical relation:

$$\Delta_{min}=(1-\cos\theta_o)^{0.22}. \tag{42}$$

Similarly, Eq. (41) for MWR can be represented by the following empirical relation in terms of Δ_{min} as follows:

$$\Gamma_{min}=0.67\Delta_{min}^{2.83}+0.26\Delta_{min}^{9.51}. \tag{43a}$$

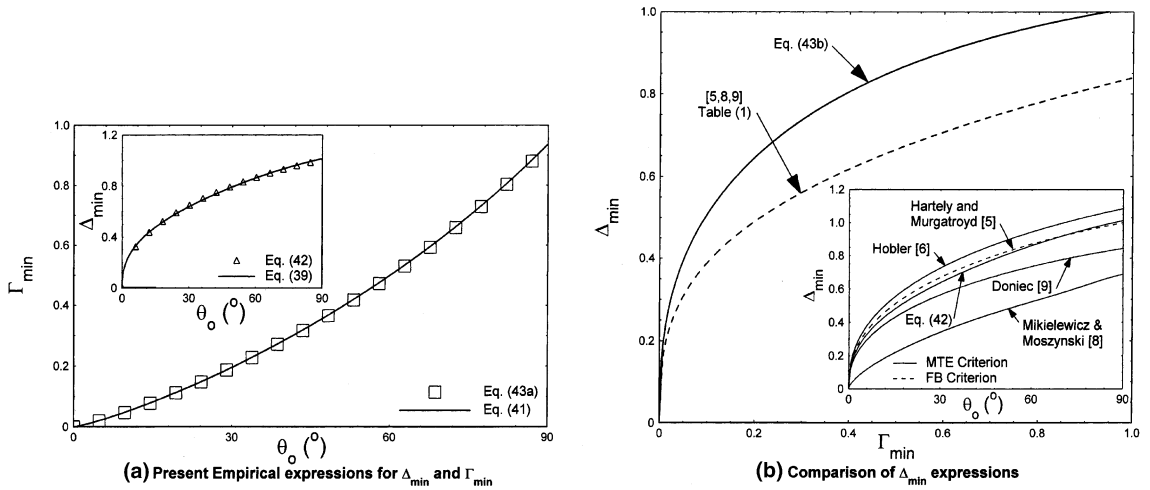

Fig. 7. Comparisons of present expressions of the MWR and MLFT with other expressions based on the FB and MTE criteria.

This equation can also be written as

$$\Delta_{\min} = 1.24\Gamma_{\min}^{0.375} - 0.228\Gamma_{\min}^{1.25}. \quad (43b)$$

Fig. 7(a) shows that the derived expressions for MLFT and MWR based on the MTE criterion (Eqs. (39) and (41)) are in excellent agreement with the empirical relations given by Eqs. (42) and (43a), respectively. In addition of being simple, the latter can be used to accurately predict MWR ($\Gamma_{\min}$) and MLFT ($\Delta_{\min}$) for a stable dry patch and the breakup of thin films of pure liquids and liquid mixtures. For a surface rewetting, Eqs. (42) and (43a) can also be used to predict MLFT and MWR, by substituting the advancing contact angle, θ_A, for θ_o, as shown later.

It is worth noting that the present empirical relation for $\Gamma_{\min}$ (Eq. (43a)) differs from those listed in Table 1 and developed based on the Nusselt theory approximation. As indicated by Eq. (42), the dependence of $\Delta_{\min}$ on the contact angle is characterized by an exponent of 0.22, instead of 0.2 in Table 1. In addition, the dependence of $\Gamma_{\min}$ on either $\Delta_{\min}$ or the contact angle is characterized by the exponents 2.83 and 9.51 on the right-hand side of Eq. (43a), versus only an exponent of 3.0 in Table 1. Note also that the coefficients in Eq. (43a) are different from 1.693 listed in Table 1.

Fig. 7(b) compares the present empirical relation for $\Delta_{\min}$ as a function of $\Gamma_{\min}$ (Eq. (43b)) with the reported expression by previous investigators based on either the FB criterion [5] or the MTE criterion using a zero-order velocity approximation [8,9] (Table 1). The reported relationship for $\Gamma_{\min}$ in terms of $\Delta_{\min}$ by various investigators is identical (Table 1), since it is developed based on the Nusselt theory approximation. Fig. 7(b) shows that the relation listed in Table 1 under predicts $\Delta_{\min}$, relative to the present expression (Eq. (43b)). The insert in Fig. 7(b) compares the present expression for $\Delta_{\min}$, Eq. (42), as a function of the equilibrium contact angle, with the expressions listed in Table 1. Despite the large difference between the present predictions of $\Delta_{\min}$ as a function of $\Gamma_{\min}$, and those of the other investigators in Table 1, the present expression of $\Delta_{\min}$ as a function of θ_o (Eq. (42)) is close to that of Hartely and Murgatroyd [5], based on the FB, but lower than that of Hobler [6], based on the MTE criterion (Table 1). The expressions of Doniec [9] and Mikielewicz and Moszynski [8], based on the MTE are much lower than the present expression (Eq. (42)).

In the next section, the present predictions of the MWR and MLFT are compared with reported experimental data for water and glycerol–water mixtures and with those calculated from the MWR measurements, respectively.

6. Comparison with experimental data

The reported data for the MWR are limited and no data are found on direct measurements of the MLFT. Most of the reported MWR data are for water on stainless steel, glass, copper, and Perspex surfaces and for a stable dry patch condition (Figs. 1 and 2). Several data points have been reported for the breakup of a thin liquid film and the rewetting of a previously dry patch by water and glycerol–water mixtures [2]. Before presenting the comparison with experimental measurement, the next section discusses the reported measurements of the contact angle for different liquids/surface material combinations.

6.1. Contact angle

The accuracy of predicting the MLFT and the MWR strongly depends on the accuracy of measuring or selecting the appropriate contact angle. The value of the contact angle depends not only of the liquid type and surface material, but also on the cleanliness, roughness, and the preparation method of the surface. Fig. 8(a) shows the dependence of the measured equilibrium contact angle of water on stainless steel (SS) [1,13] and Fig. 8(b) compares the measured advancing and equilibrium contact angles for glycerol–water mixtures on glass [14]. The contact angle of water on SS decreases with surface roughness reaching a minimum at 2.0 μm, then increases with further increase in surface roughness. The values of the equilibrium contact angle, θ_o, used in the present predictions of the MWR and MLFT for a stable dry patch (Fig. 9) are based on the data in Fig. 8(a) and (b), in addition to those reported by the individual authors in their experiments.

For the prediction of the breakup of a thin, continuous liquid film falling down a vertical surface, Ponter et al. [1] have reported insignificant differences in the measured values of the dynamic receding contact angle, θ_{dR}, and θ_o for ethanol–water mixtures on Perspex at 293 K (Fig. 8(c)). Therefore, for the breakup of a flowing, isothermal, thin liquid film θ_o is used in predicting the MWR and MLFT using the present expressions (Eqs. (39), (41), (42), (43a), (43b)). For the rewetting condition, the advancing contact angle, θ_A, in Fig. 8(b) is substituted for θ_o in the present expressions of the MWR and MLFT (Eqs. (39), (41), (42), (43a), (43b)) for glycerol–water mixtures. In the following sections, the present predictions of the MWR are compared with the reported data by various investigators for water and glycerol–water mixtures.

6.2. Comparison with the water data of MWR for a stable dry patch

Ponter et al. [1] have conducted a series of experiments to measure the MWR for the formation of a stable dry patch, following the breakup of thin films of water and ethanol–water mixtures flowing down on the outside surface of vertical tubes made of copper, stainless steel, Perspex, and carbon. They investigated the effects of the absorption of ethanol–air mixtures into water on the MWR for different tube lengths (0.3 and 1.2 m), surface roughness, and temperatures from 293 to 328 K. In addition, they measured the equilibrium contact angle at these temperatures. Fig. 9(a) compares the MWR calculated using Eqs. (41) or (43a) with the reported measurements of water by Ponter et al. [1] for a stable dry patch. As show in this figure, the present predictions are in good agreement with the data, to within ±20%. The measurements of the MWR in this figure are for a water film on different surface materials (stainless steel, copper, and Perspex) at 293–323 K and for equilibrium contact angles of 66°–87°. As shown in

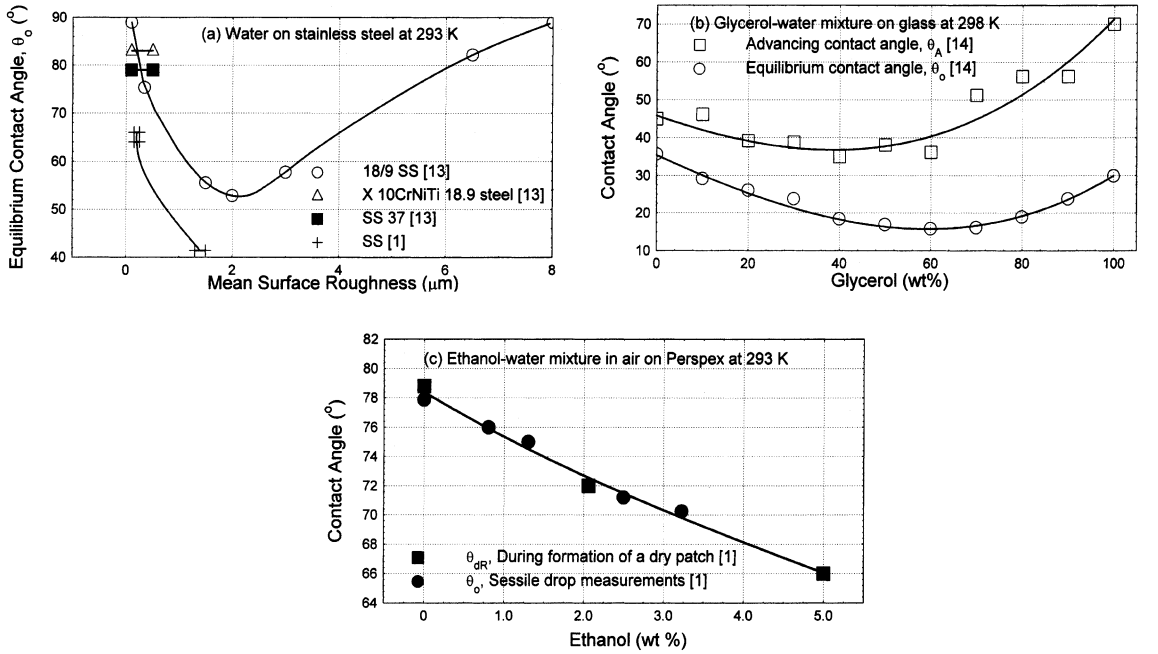

Fig. 8. Reported measurements of the contact angles for different liquids/surface materials.

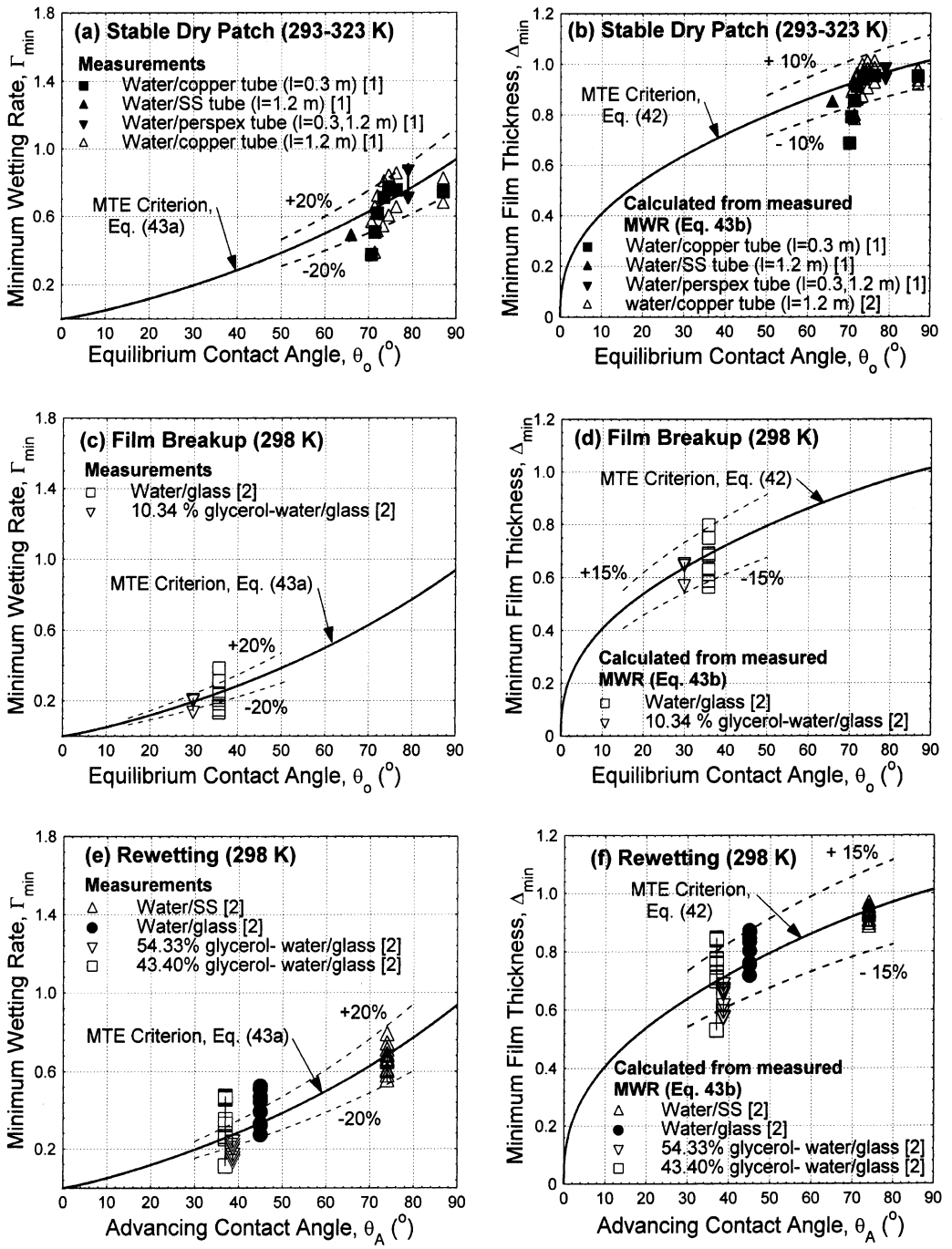

Fig. 9. Comparison of present predictions of the MWR and MLFT with the data for water and glycerol–water mixtures.

Fig. 9(a), there is a large scattering in the reported measurements of the MWR, even in the same experimental setup [1]. This scattering is due to the uncertainties in the measurements of both the MWR and the equilibrium contact angle, θ_o. In a recent study, Bernardin et al. [15] have shown that the contact angle is highly influenced by the surface finish and the presence of impurities on the surface. They have also shown a wide spread in the measured values of the contact angle, which was attributed to surface contamination.

The present predictions of the MLFT of water are also in good agreement with the values calculated from the measurements of the MWR by Ponter et al. [1] for a stable dry patch (Fig. 9(b)). As shown in this figure, the present predictions of the MLFT are within ±10% of most of the calculated values.

6.3. Comparison of the MWR and MLFT at the breakup of a thin liquid film

Munakata et al. [2] have conducted a series of experiments to measure the minimum wetting rate at the breakup of thin films of water and glycerol–water

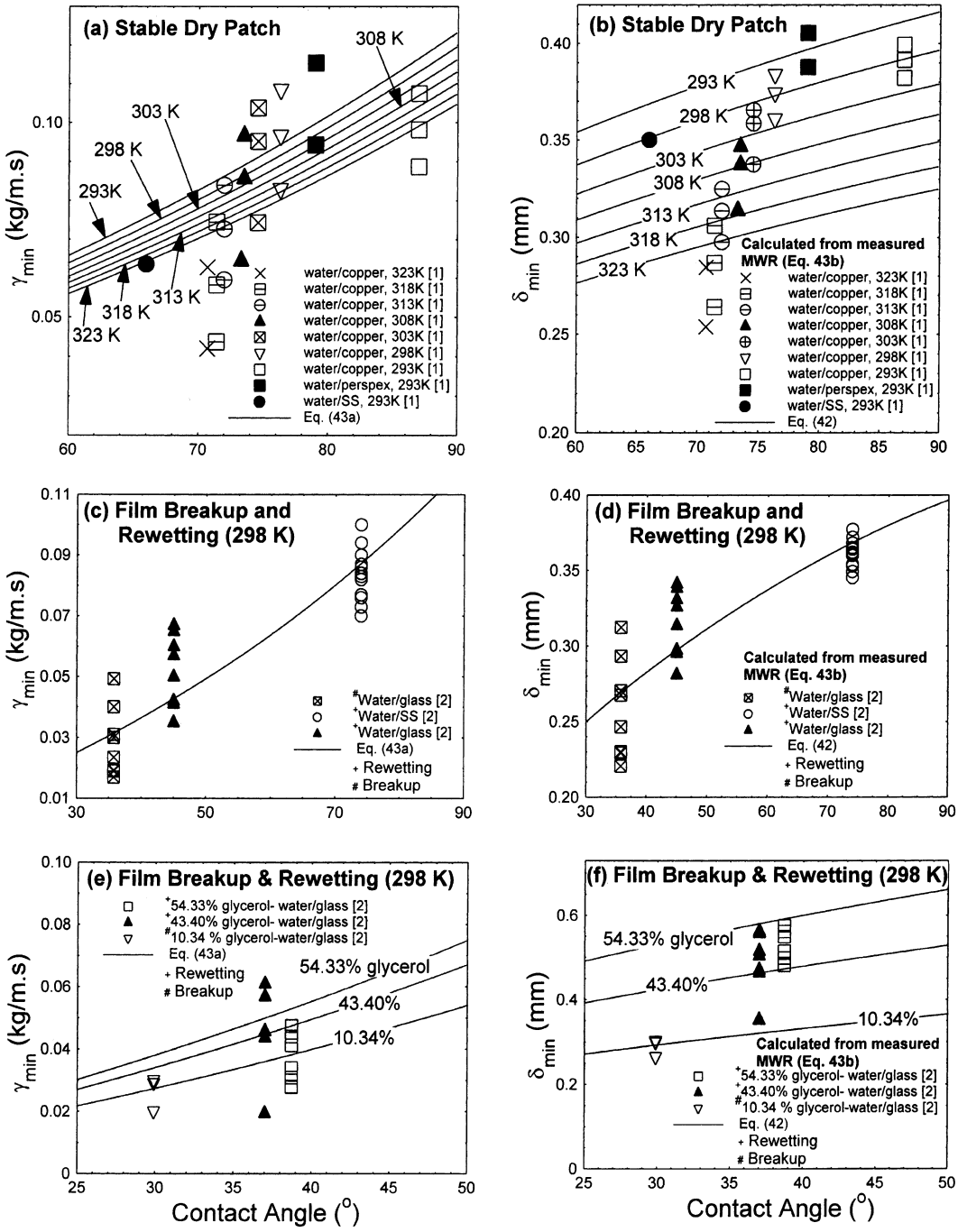

Fig. 10. Predictions of the γ_{min} and δ_{min} for water and glycerol–water mixtures.

mixtures on glass at room temperature (298 K). They also measured the MWR for rewetting a previously dry surface. They used six tubes made of glass and stainless steel. The tubes had an outer diameter of 3.4 cm and length of 15 cm, but different shapes at the top of the wall (see Fig. 1 in their paper). As indicated in Fig. 9(c) the present predictions of the MWR are within ±20% of the reported date for water and 10.34 wt% glycerol–water mixture [2]. The calculated values of the MLFT from the MWR measurements [2] are also in good agreement with the present predictions (Eq. (42)), to within ±15% (Fig. 9(d)).

6.4. Comparison of the MWR and MLFT for the rewetting of a dry surface

In the experiments of Munakata et al. [2], the liquid flow rate was increased until the surface was covered completely by a thin, continuous liquid film, which they referred to as "case II". The measured liquid flow rate in this case is the MWR for rewetting the surface. The reported measurements of the MWR are compared in Fig. 9(e) with the present predictions after substituting the advancing contact angle, θ_A, for the equilibrium contact angle, θ_o, in Eqs. (41) or (43a). The predictions agree with the experimental data to within ±20%. The present predictions of the MLFT are also in good agreement with the calculated values from the reported MWR measurements [2], to within ±15% (Fig. 9(f)).

Fig. 10(a) compares the measurements of the minimum wetting rates, γ_{min}, of water on copper, SS, and Perspex at different temperatures, as a function of the equilibrium contact angle, with the present predictions (Eq. (43a)). Fig. 10(b) compares the corresponding values of the minimum liquid film thickness, δ_{min}, with the present predictions. Similar comparisons of the data for the breakup of thin films of water on SS and glass and for rewetting these surfaces at 298 K are shown in Figs. 10(c) and (d). Figs. 10(e) and (f) show similar comparisons for glycerol–water mixtures on glass at 298 K. An examination of the results in Fig. 10(a)–(d) reveals that for the same equilibrium contact angle and temperature, the values of the minimum wetting rate and the corresponding minimum liquid film thickness for a stable dry patch and for the breakup of liquid films are identical, as indicated earlier. These figures also show that for water, the minimum film thickness ranges from ~0.25 to 0.42 mm, depending on the type of the solid surface, temperature, and the contact angle. For water–glycerol mixtures, the values of the minimum liquid film thickness for a glass surface vary from ~0.27 to 0.65 mm, depending on the fraction of the glycerol in the mixture and the contact angle.

7. Summary and conclusions

Analytical expressions for the MLFT and the corresponding MWR for a stable dry patch following the breakup of a thin, isothermal liquid film flowing down a vertical surface are developed using the MTE criterion. The MTE criterion has been applied to a stable, flowing liquid rivulet, whose total energy is the sum of the kinetic energy and the interfacial energies at L–S and L–V interfaces. The kinetic energy is determined using the obtained approximate analytical expression of the two-dimensional velocity distribution in the rivulet obtained using the Ritz method. For a liquid rivulet characterized by $\theta_o = 45°$ and $\varepsilon = 0.168$, the present velocity distribution is in excellent agreement with the numerical solution of Allen and Biggin [11]. In addition to the velocity distribution, the derived analytical expression for the profile of the liquid rivulet is incorporated into the total energy equation of the rivulet. The minimization of the total energy gave analytical expressions for both the MLFT and MWR (Eqs. (39) and (41)). These expressions are accurately represented by the empirical relations in Eqs. (42) and (43a), respectively.

The present predictions of the MWR for a stable dry patch are in good agreement, to within ±20%, with measurements for water on several surfaces at temperature of 293–323 K. The calculated values of the MLFT from the measurements of the MWR are also in good agreement with the present predictions (Eqs. (39) or Eq. (42)), to within ±10–15%. Results showed that the MWR and the corresponding MLFT for a stable liquid rivulet are the same as at a film liquid breakup. In addition, the results confirmed the validity of the present predictions of the MWR and MLFT (Eqs. (39) and (41)) for the rewetting condition, after substituting the advancing contact angle for the equilibrium contact angle.

Acknowledgements

This research is funded by the University of New Mexico's Institute for Space and Nuclear Power Studies.

References

[1] B. Ponter, G.A. Davies, T.K. Ross, P.G. Thornley, The influence of mass transfer on liquid film breakdown, Int. J. Heat Mass Transfer 10 (1967) 349–359.
[2] T. Munakata, K. Watanabe, K. Miyashita, Minimum wetting rate on wetted-wall column, J. Chem. Eng. Jpn. 8 (6) (1975) 440–444.
[3] F.E. Andros, Heat transfer characteristics of the two-phase closed thermosyphon (wickless heat pipe) including direct

flow observation, Ph.D. Dissertation, Arizona State University, Tempe, AZ, 1980.
[4] S. Roesler, M. Groll, Flow visualization and analytical modeling of interaction phenomena in closed two-phase flow systems, in: Proceeding of the Eighth International Heat Pipe Conference, Beijing, China, Institute of Engineering Thermophysics, Chinese Academy of Sciences, 1992, pp. 26–32.
[5] D.E. Hartely, W. Murgatroyd, Criteria for the break-up of thin liquid layers flowing isothermally over solid surface, Int. J. Heat Mass Transfer 7 (1964) 1003–1015.
[6] T. Hobler, Minimum surface wetting, Chemia Stosow 2B (1964) 145–159.
[7] S.G. Bankoff, Minimum thickness of a draining liquid film, Int. J. Heat Mass Transfer 14 (1971) 2143–2146.
[8] J. Mikielewicz, J.R. Moszynski, Minimum thickness of a liquid film flowing vertically down a solid surface, Int. J. Heat Mass Transfer 19 (1976) 771–776.
[9] A. Doniec, Laminar flow of a liquid rivulet down a vertical solid surface, Can. J. Chem. Eng. 69 (1991) 198–202.
[10] J.N. Reddy, An Introduction to the Finite Element Method, McGraw-Hill, New York, 1984.
[11] R.F. Allen, C.M. Biggin, Longitudinal flow of a lenticular liquid filament down an inclined plane, Phys. Fluids 17 (2) (1974) 287–291.
[12] M.J. Forry, Variational Calculus in Science and Engineering, McGraw-Hill, New York, 1968.
[13] E. Krell, The solid-liquid boundary in chemical engineering, Br. Chem. Eng. 12 (4) (1967) 562–567.
[14] A.B. Ponter, A.P. Boyes, The rupture of isothermal vertical liquid films, J. Chem. Eng. Jpn. 5 (1) (1972) 80–83.
[15] J.D. Bernardin, I. Mudawar, C.B. Walsh, E.I. Franses, Contact angle temperature dependence for water droplets on practical aluminum surfaces, Int. J. Heat Mass Transfer 40 (5) (1997) 1017–1033.